AIAA JOURNAL
Vol. 37, No. 1, January 1999

Microfabricated Shear Stress Sensors, Part 1: Design and Fabrication

Tao Pan,* Daniel Hyman,† Mehran Mehregany,‡ Eli Reshotko,§ and Steven Garverick¶
Case Western Reserve University, Cleveland, Ohio 44106

The design and fabrication of shear stress sensors based on the floating-element method and polysilicon-surface-micromachining technology is reported. Three designs have been developed for microfabrication, two including monolithic integration of mechanical sensor elements with on-chip circuitry. The first design is a four-mask standard polysilicon-surface-micromachining process to develop passive floating-element sensors with optically determined deflection sensitivity. The second-generation devices are fabricated in a six-mask modified N-channel metal-oxide-semiconductor process, where sensor elements and signal conditioning circuitry have been integrated on the sensor die for amplified voltage output. The third design modifies the commercially available micromachined by replacing the accelerometer element with a shear-stress-sensitive floating element, enabling active sensing for linear response and self-test features.

I. Introduction

A. Shear Stress and Its Measurement

ADVANCES in fluid mechanics require effective instrumentation for studying flow. A parameter that has been difficult to measure directly and locally in wind-tunnel instrumentation is wall shear stress—the topic of the sensor development in this work. This paper presents the design and fabrication of floating-element microfabricated shear stress sensors, and Ref. 1 describes their testing and calibration.

An object exposed to a flow experiences on its surface a shear force due to the viscosity of the fluid as suggested in Fig. 1. The shear force per unit area is the shear stress τ_w, which is related to the flow velocity profile by

$$\tau_w = \left(\mu \frac{\partial u}{\partial y}\right)_{y=0} \tag{1}$$

where μ is the viscosity of the fluid evaluated at the surface temperature. Knowledge of the shear stress is of primary importance in aerodynamic and hydrodynamic design because it determines a major part of the aerodynamic drag. Shear stress also plays a critical role where the performance of an aerodynamic component is limited by flow separation, including, for example, aircraft stall. However, shear stress is not an easy quantity to measure, and although no universal solution exists for accurate determination of wall shear stress for every situation, several techniques have been developed. These techniques are divided into two main categories, indirect and direct, according to the nature of the measuring method.[2,3] Indirect methods include Stanton tube/razor blades, Preston tubes, heated-surface wires, heated-surface film elements, and liquid surface tracing. The only technique qualifying as a direct measurement of shear stress is the floating-element technique, which is pursued in this work. With direct measurement, no assumptions have to be made to relate the shear stress to the measured quantities.

Figure 1 (see Ref. 4) is a schematic representation of the floating-element method of direct shear stress measurement. The shear force exerted by the fluid flow on the surface of the floating element is balanced by the restoring force of the spring. Thus, the displacement of the floating element δ is directly related to the shear stress τ_w by

$$k\delta = A\tau_w \tag{2}$$

where k is the spring constant of the system and A is the area of the floating element. These two values determine the sensitivity and shear stress range of the device.

B. Microelectromechanical Systems and Surface Micromachining

Microelectromechanical systems (MEMS) are a growing field of research centered on the development of sensors and actuators using semiconductor processing techniques. A fundamental aspect of MEMS is the use of integrated circuit fabrication techniques to define mechanical elements in addition to electrical elements on the same substrate using thin-film materials or the substrate itself. Microfabrication confers a number of advantages over discrete component machining and assembly due to the nature of batch processing increasing dimensional control and production output. Sensor repeatability and precision are maximized because the photolithographic process that defines the sensor elements has micron resolution and identical processing is performed for large numbers of devices. The resultant devices can be produced at reduced cost because large numbers can be created with fewer discrete assembly and device-specific calibration steps. MEMS devices also enable the ability to integrate sensors with signal processing circuitry on the same substrate, increasing the functionality of devices without substantially increasing costs.

The key technology for the fabrication of MEMS devices is called micromachining, i.e., the technology to sculpt silicon into desired microstructures. There are several micromachining process technologies,[5,6] one of the most prominent of which is surface micromachining, which is used for the shear stress sensor development in this work.

As will be discussed later, surface micromachining employs sequential deposition and patterning of thin films on a substrate to form the desired microstructures. Some layers are patterned into the structural components, whereas other layers are used temporarily as sacrificial spacers. In the final stage of the process, the wafer is immersed in a chemical etchant to dissolve the sacrificial layers, releasing the structural components.

MEMS confers additional advantages in fluid flow research because of the potential for small device sizes. Because the boundary-layer thicknesses in fluid flows can be on the order of millimeters, and turbulent boundary-layer structures on the order of hundreds of microns, small device sizes are needed to avoid disturbance of the

Received Dec. 3, 1997; revision received July 2, 1998; accepted for publication July 13, 1998.

*Graduate Research Assistant, Department of Electrical Engineering and Applied Physics; currently Project Manager, Advanced MicroMachines, Inc., 11000 Cedar Avenue, Cleveland, OH 44106.

†Research Assistant, Department of Electrical Engineering and Computer Science, and Hughes Fellow, Hughes Research Laboratories.

‡George S. Dively Professor of Engineering, Department of Electrical Engineering and Computer Science.

§Kent H. Smith Professor of Engineering, Department of Mechanical and Aerospace Engineering. Fellow AIAA.

¶Associate Professor, Department of Electrical Engineering and Computer Science.

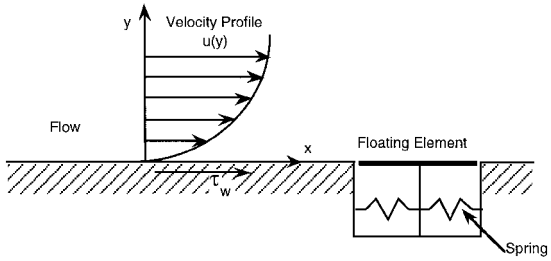

Fig. 1 Schematic description of flow velocity profile and shear stress on a surface.[4]

boundary layer and to avoid spatial averaging of small flow structures. MEMS sensors with physical sizes on the order of tens or hundreds of microns would not significantly disturb boundary layers and would come close to the ability to take a measurement at a point.

C. Microfabricated Floating-Element Shear Stress Sensors

Using MEMS technology, researchers have pursued the development of floating-element shear stress microsensors, including the leading work of Schmidt[4] and Schmidt et al.[7,8] A square floating element with four tether suspension beams was microfabricated in 30-μm-thick polyimide, which deflected laterally under applied shear stress perpendicular to the tether axis. Electrodes were patterned into the polyimide floating element and on the substrate surface below to provide a differential capacitance measurement scheme. Before polyimide patterning, N-channel metal-oxide-semiconductor (NMOS) transistors were fabricated into the silicon substrate to provide signal amplification and to convert capacitance change to an output voltage.

Floating-element shear stress sensor work has continued under Shajii et al.[9] and Padmanabhan et al.[10] with the use of wafer bonding and etch-back micromachining. In this type of microfabrication, the devices are defined in a thin layer of silicon on the surface of a substrate that is bonded to the face of another substrate and thinned back to the desired thickness of the device elements. The device is then patterned and other fabrication steps completed for the sense elements before release as described earlier. Two sensors have been designed with this method by Shajii et al.[9] and Padmanabhan et al.[10] with the benefit of superior material properties of single-crystal silicon as compared with polyimide. One device incorporates a piezoresistive measurement scheme for operation under high stress conditions up to 12 kPa (Ref. 9) for measurement in polymer extrusion processes. The latest work,[10] for low shear stress applications, incorporates a nonobtrusive optical measurement scheme with photodiodes that substitute the problems associated with electrical connections with those of optical access to sensors throughout implementation.

Other work in micromachined shear stress sensors has progressed with the development of hot-element devices by Liu et al.[11] and Huang et al.[12,13] Micromachining enables very small, precise dimensions for these elements and makes the fabrication and testing of arrays of sensors achievable with nominal incremental complexity. In addition to accuracy with fabrication, small size and cavity micromachining allows very high sensitivities with very small time constants of measurement.[12,13] The conventional limitations of calibration of hot-element shear stress sensors remain, however, and so the direct measurement technique is chosen in the present work.

The shear stress sensors discussed in this paper are floating-element sensors that use heavily phosphorus-doped polysilicon as the structural material instead of polyimide. They are designed for low shear stress applications (up to 40 Pa) and use optical and capacitive measurement schemes. Attention has been given to reduce the perturbation of the surface flow, building on the early designs of Schmidt[4] and Schmidt et al.,[7,8] by using smaller sensor elements and active sensor operation. In addition, polyimide absorbs water from the ambient in proportion to the relative humidity that, as well as the polyimide's viscoelastic property, results in long-term instability of sensor structural material and output drift. Polysilicon was chosen in our work because it is a stable material with superior mechanical characteristics. The size of a polysilicon floating element can be made an order of magnitude smaller for similar shear stress ranges, and the fabrication process is simplified due to its semiconductive properties.

II. Transducer Element Design

Three different designs have been developed in this work, varying floating-element geometry and sensor output. The first-generation Case Western Reserve University (CWRU) sensor is designed in a four-mask standard polysilicon surface-micromachining process to develop passive floating-element sensors with optically determined deflection. Because of the limitations of optical measurements of micron-scale deflection, the second-generation CWRU devices are fabricated in a six-mask modified NMOS process, where sensor elements and signal conditioning circuitry have been integrated on the sensor die for amplified voltage output. The third design modifies the commercially available micromachined Analog Devices, Inc., accelerometers (ADXL) by replacing the accelerometer element with a shear-stress-sensitive floating element, enabling active sensing for linear response and self-test features. The floating element and electrical sensing scheme in these devices functions similarly to that of the second-generation CWRU devices, but the signal-conditioning circuitry provides linear voltage output with shear stress and incorporates a self-testing function.

A. First-Generation Sensor Design

The transducer elements of the shear stress sensors developed in this paper are based on polysilicon-surface-micromachined lateral resonant structures with folded beam suspensions as shown in Fig. 2. These devices take advantage of the fact that folded beam suspensions relieve internal residual stresses of the structural polysilicon material and are more flexible than simple four-beam suspensions used in earlier microfabricated shear stress sensor designs, allowing for greater sensor sensitivity. Lateral resonant structures are used as transducing elements in various other microsensors and microactuators and are well characterized.[14–16] After etching the sacrificial layer, the thin-film internal stresses normally play important roles in beam deflection characteristics, but because these stresses are relaxed in folded beam structures, predictable sensor characteristics result.

When a force F (e.g., resulting from shear stress) is applied to the floating element, it will cause the beams to bend, resulting in a displacement δ as illustrated schematically in Fig. 3. The force is divided among the four folded suspension beams that, assuming that the outer connecting truss is rigid, deflect according to beam theory as[16]

$$x(y) = [(F/4)/(12EI)](3Ly^2 - 2y^3) \tag{3}$$

for $0 \le y \le L$, where L is the length of beam, E is Young's modulus of polysilicon, and I is the moment of inertia of the beam. From Fig. 3, the segment is deflected by $\delta/2$ at B, and so $x(L) = \delta/2$. Then

$$(\delta/2) = [(F/4)/(12EI)]L^3 \tag{4}$$

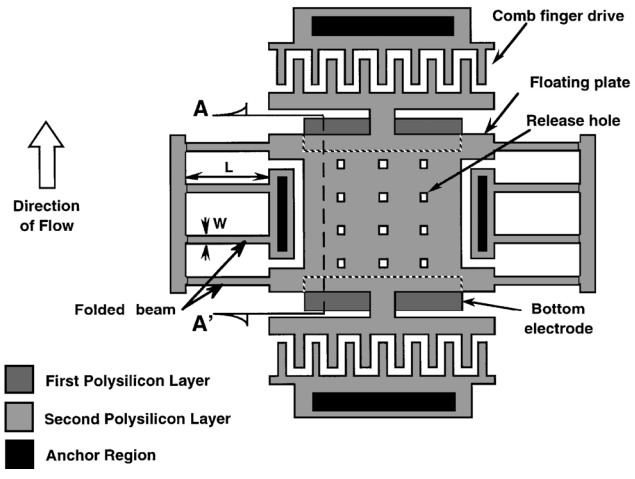

Fig. 2 Lateral resonant structure with folded-beam suspension.

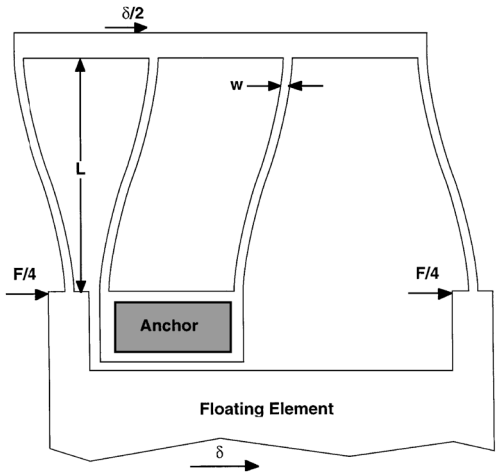

Fig. 3 Deflection shape of the folded-beam suspension.[16]

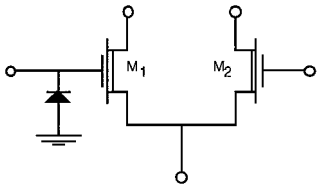

Fig. 4 On-chip differential-pair amplifier.

and because $I = \frac{1}{12} t W^3$, we have

$$\delta = (F/2Et)(L/W)^3 \tag{5}$$

where t and W are the thickness and width of the beam, respectively. The spring constant K of the folded beam structure is then defined as

$$K = (F/\delta) = 2Et(W/L)^3 \tag{6}$$

Forces other than that caused by wall shear stress also act on the floating element, as noted by Schmidt and others. These additional forces include the shear stress of fluid flowing underneath the floating element and also the gauge force caused by the pressure difference between the leading and trailing edges of the element. These additional forces are discussed in detail in the following paper on calibration,[1] rather than the present design paper, because these forces are small, on the order of a few percent of the shear stress forces. They are both dependent on the element and gap thicknesses, respectively, which in microfabricated floating-element shear stress sensors correspond to the film thicknesses of the fabrication layers, approximately 2 μm.

B. Second-Generation Sensor Design

The second generation of the CWRU sensors includes the monolithic integration of on-chip signal amplification circuitry. Because of the small size of the devices, capacitance changes are on the order of several femtofarads, with very small signal changes on the floating plate. As a result of these small electrical signals and characteristics, device output can be lost in parasitic capacitances associated with pad contact and wire bonding. Figure 4 shows the circuit schematic of an on-chip differential amplifier. The gate of M_1 is connected to the floating element with a diode necessary to bias the NMOS transistor. The gate of M_2 is a fixed reference node, and the drains are output nodes of the differential pair. Both M_1 and M_2 are depletion-mode NMOS transistors with channel widths of 120 μm and lengths of 12 μm. The voltage gain A_v of the differential pair is

$$A_v = g_m R_d \tag{7}$$

where g_m is the NMOS transconductance, and R_d is the value of off-chip resistors connected to the drains of the devices (not shown in Fig. 4). Typical gains are about 20.

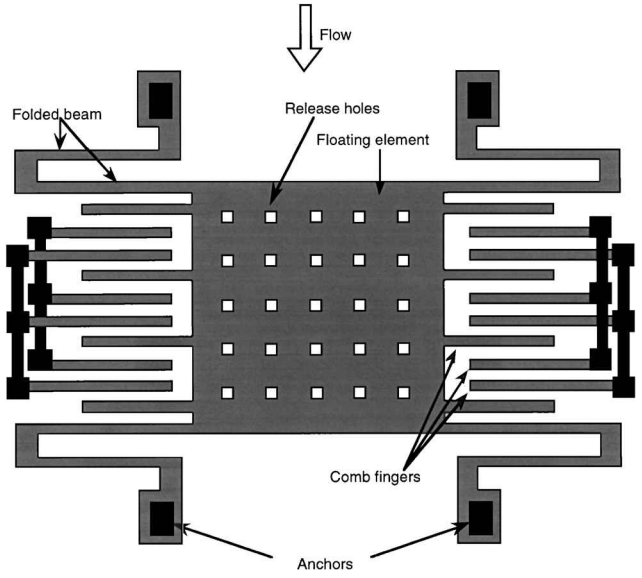

Fig. 5 Plan-view schematic of a horizontal-electrode floating element.

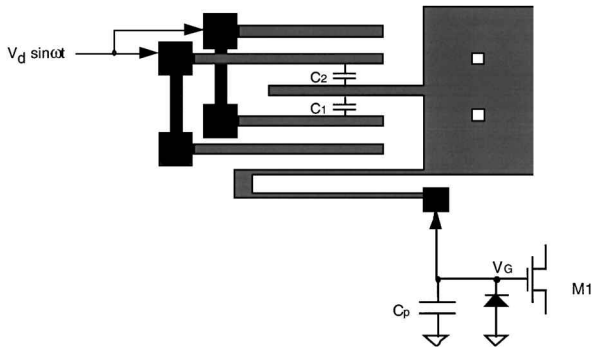

Fig. 6 Schematic illustration of the sense capacitors of shear stress sensors.

For the transducer elements shown in Figs. 5 and 6, the sense capacitors are formed by interdigitated comb fingers. When the floating element deflects under shear force, the gaps between the comb fingers change, resulting in changes of capacitance.

When the electrodes are driven with the same ac signal, the voltage that appears at the gate of the NMOS transistor M_1 is

$$\begin{aligned} v_G &= \frac{C_1 + C_2}{C_1 + C_2 + C_p} V_d \sin \omega t \approx \frac{C_1 + C_2}{C_p} V_d \sin \omega t \\ &= \frac{\varepsilon_0 t_{\text{poly}\,2} L}{C_p} \left(\frac{1}{d_0 - \delta} + \frac{1}{d_0 + \delta} \right) V_d \sin \omega t \\ &= \frac{\varepsilon_0 t_{\text{poly}\,2} L}{C_p d_0} 2 V_d \sin \omega t \frac{1}{1 - (\delta/d_0)^2} \end{aligned} \tag{8}$$

where C_p is the parasitic capacitance at the gate of M_1, where it is assumed $C_p \gg C_1 + C_2$, $t_{\text{poly}\,2}$ is the thickness of the second polysilicon layer, L is the overlap between the stationary and movable comb fingers, d_0 is the initial gap between the comb fingers, and δ is the displacement of the floating element. The output voltage is thus

$$v_G = \frac{\varepsilon_0 t_{\text{poly}\,2} L}{C_p d_0} 2 V_d \sin \omega t \frac{1}{1 - [(A/d_0 k)\tau]^2} \tag{9}$$

$$v_0 = A_1 v_G = A_1 \frac{\varepsilon_0 t_{\text{poly}\,2} L}{C_p d_0} 2 V_d \sin \omega t \frac{1}{1 - [(A/d_0 k)\tau]^2} \tag{10}$$

which is a complex function that must be determined empirically given the fabrication-dependent parameters defined earlier, and where A_1 is the voltage gain of the differential amplifier.

C. CWRU/ADI Shear Stress Sensor Design

CWRU has cooperated with Analog Devices, Inc. (ADI), to develop shear stress sensors based on the existing ADXL line of automotive accelerometers. These sensors have floating elements similar to the devices described in Sec. II.B with horizontal electrodes. These devices operate with mechanics identical to the devices discussed in the previous section, with the exception that the suspension structures are fixed-end rather than folded-cantilever beams. These devices are additionally operated in an active configuration such that the floating element does not move throughout sensor operation, assuring linearity throughout the sensor range.

When subjected to fluid flow, the shear force displaces the floating plate, causing the plate electrodes to move closer to one set of fixed electrodes and away from the other. The two capacitances formed by the movable and fixed electrodes change accordingly, C_1 increasing and C_2 decreasing as shown in Fig. 6. The drive electrodes are operated with a balanced differential stimulus, and charge accumulates on the plate due to the capacitance mismatch, which is measurable as plate voltage:

$$V = \frac{C_2 - C_1}{C_2 + C_1} V_i = \frac{\delta}{d} V_i \tag{11}$$

where δ is the deflection, d is the initial gap between comb fingers, and V_i is the magnitude of the driving signal, with parasitic capacitance neglected. The drive configuration for the CWRU/ADI sensors results in a nominal zero output with matched capacitances unlike the output voltage of the CWRU second-generation sensors. In these devices, a 1-MHz, 600-mV carrier signal drives the sense electrodes similar to the driving discussed for the CWRU devices, but with square waves and complimentary signals sent to each pair of electrodes rather than synchronous ac driving, resulting in an expected linear output with respect to shear stress. Parasitic capacitance C_p only affects loop gain, which has been made high enough to obtain accurate force balancing independent of the exact value of C_p.

On-chip circuitry provides force-balance sensor operation.[17,18] The floating-element voltage signal is demodulated by an externally referenced oscillator and fed into a preamplifier as shown in Fig. 7. This signal is fed back to the stationary electrodes as a bias signal. This bias incites an electrostatic force to attract the floating towards the far electrode and away from the near electrode. Electrostatic forces in these devices are attractive only, such that the net attractive force causes the floating element to move back to its zero displacement position. This mode of sensor operation is called force-balance operation, and with the advantage of not moving under shear stress, surface flow perturbations are minimized with noise and distortion reduced accordingly. Also, the response is more linear due to operation in this mode.

Figure 7 also shows a schematic of the external electrical connections to the sensor. The input voltage is +5 V, with external capacitors of 22, 22, and 10 μF for C_1, C_2, and C_3, respectively. Incorporated into the sensor's force-balance operation is a self-test feature that applies a voltage at Stest to the stationary electrodes to simulate a scaled shear force on the floating element.[17,18] This self-test feature can be used to ensure proper sensor operation. The preamplifier output Vpr can be used for measurement because the signals sent back to the floating element are in the millivolt range and large enough to obtain accurate readings. The amplified output Vout can be used to obtain measurements up to the saturation limit around 4 V. Some of the resistors in the preamplifier are laser trimmed at ADI to increase sensitivities and to match sensor-to-sensor output.

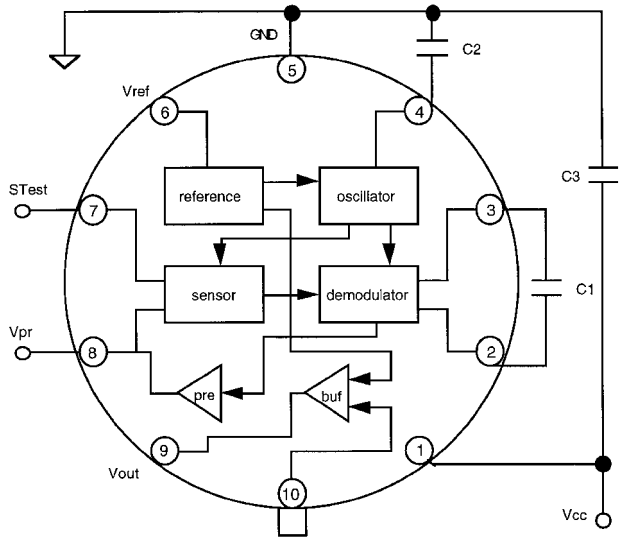

Fig. 7 External electrical connections to CWRU/ADI sensor.[17]

III. Sensor Fabrication

A. First-Generation CWRU Sensors

The first-generation CWRU sensor is fabricated in a four-mask, polysilicon-surface-micromachining process schematically illustrated in Fig. 8. The process starts with a bare silicon wafer with a layer of thermally grown silicon dioxide to release the stress between the substrate and the following layer. A silicon nitride layer is deposited to insulate devices from the substrate (Fig. 8a). The first polysilicon layer (0.5 μm) is then deposited and heavily doped to improve conductivity, then patterned to form a shield and bottom electrodes (Fig. 8b). A sacrificial oxide layer (2.2 μm) is deposited on top of the first polysilicon layer and patterned for bushing molds (0.5 μm deep) that form small bumps at the bottom of the second polysilicon layer to prevent the floating element from touching the lower electrodes (Fig. 8c). Anchor areas are also patterned where oxide is completely etched away (not shown in Fig. 8). The anchors provide mechanical support for the polysilicon structures and enable electrical connection between the two polysilicon layers. The second polysilicon layer (2.2 μm) is then deposited and heavily doped with phosphorous. The floating element and suspension are defined in Fig. 8d. The devices are then immersed in HF (49% by weight) to etch the sacrificial oxide, freeing the

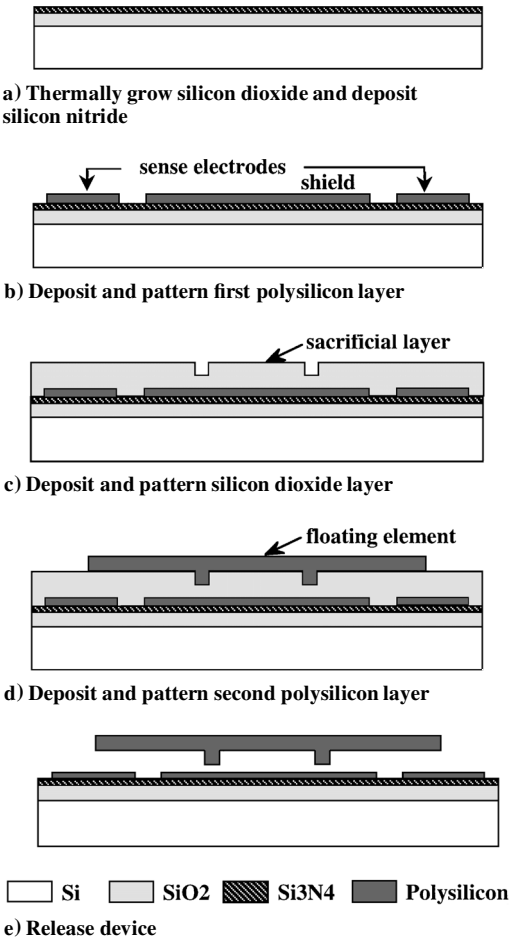

Fig. 8 CWRU shear stress sensor fabrication process (cross section A-A′ in Fig. 2).

polysilicon floating elements (Fig. 8e). A scanning-electron microscope/micrograph (SEM) picture of the fabricated sensor is shown in Fig. 9. Further discussion of the release process is presented in Ref. 1.

B. Second-Generation CWRU Sensors

The fabrication process for the integrated shear stress sensors is outlined next and schematically illustrated in Fig. 10. The integrated sensor process starts with ⟨100⟩ p-type silicon wafers with a boron concentration of 1×10^{16} cm^{-3}. A 400-Å-thick silicon dioxide layer is grown in dry oxygen at 1000° C (Fig. 10a); the SiO_2 layer serves as a buffer to relieve the mechanical stress due to unequal thermal expansion of the silicon substrate and the silicon nitride layer, which is subsequently deposited as an insulating layer. The first low-pressure chemical vapor deposition (LPCVD) silicon nitride layer (1200 Å in thickness) is then deposited. This shared layer serves two functions. First, it acts as a shield to prevent oxidation of the active area during field oxide growth. Second, it serves as an insulating layer between the bottom electrodes of the transducer elements and the silicon substrate. The nitride layer is then patterned to define the active areas of the wafer in the circuit region (Fig. 10a).

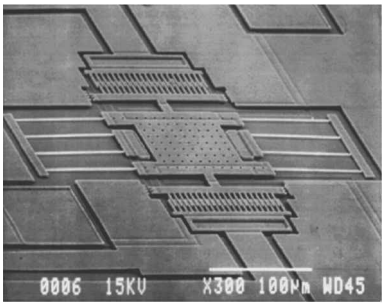

Fig. 9 SEM picture of CWRU shear stress sensor with 100-μm beam.

A field threshold adjust implantation of boron was performed next at an energy of 100 KeV and a dosage of 6×10^{12} atoms/cm^{-2}. The implantation is masked from the active area by the nitride layer defined in the previous step. Then a 0.6-μm field oxide is grown at 950° C to isolate the active area from neighboring active areas (Fig. 10b). Note that no oxide grows in the sensor regions due to the nitride layer that is present. Next, the remaining nitride layer in the circuit area is removed by reactive-ion etch (RIE) etching (Fig. 10b). Arsenic (65 KeV, 2×10^{12} cm^{-2}) is then implanted into the active area to adjust the threshold voltage of the NMOS transistors. The remaining pad oxide serves as a blocking layer to minimize implantation damage to the silicon substrate.

After arsenic implantation, the pad oxide is removed in buffered HF to expose the silicon substrate in the active area for gate oxidation (Fig. 10c). A high-quality silicon dioxide film (400 Å) is grown in a dry oxygen environment and is used as the gate oxide for the metal-oxide-semiconductor field-effect transistors (MOSFETs) (Fig. 10c). After gate oxidation, the first polysilicon layer (0.5 μm) is deposited by LPCVD at 610° C and heavily doped with phosphorus by diffusion from solid sources at 875° C for 90 min. The

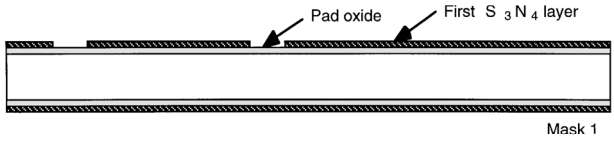

a) Grow pad oxide and deposit and pattern first silicon nitride layer

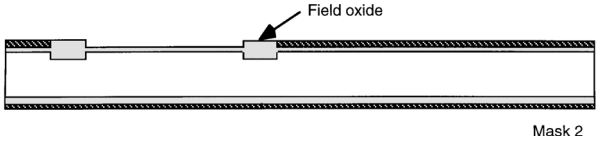

b) Grow field oxide and remove nitride from active area

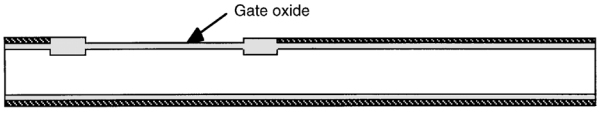

c) Remove pad oxide from active area and replace with grown gate oxide

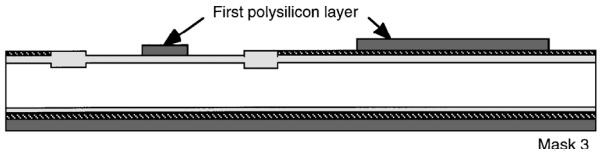

d) Deposit and pattern the first polysilicon layer

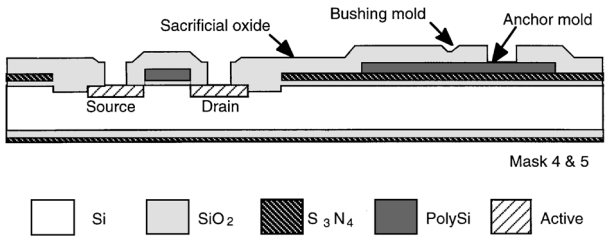

e) Implant active regions, then deposit sacrificial oxide and open bushing molds, anchor, and contact areas, followed with a backside strip

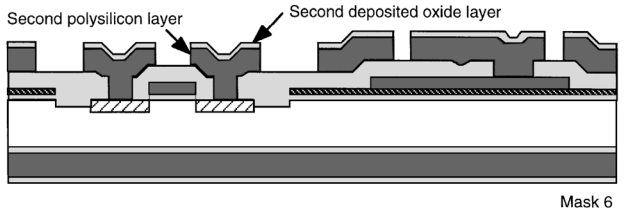

f) Deposit and pattern the second polysilicon layer and low-temperature oxide layer

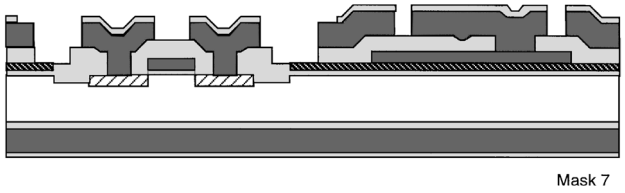

g) Remove the oxide layers around circuit area

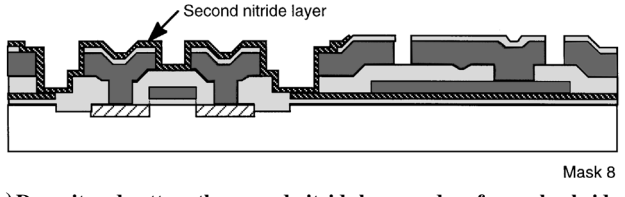

h) Deposit and pattern the second nitride layer and perform a backside strip

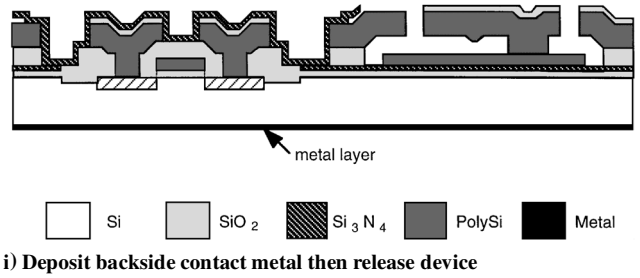

i) Deposit backside contact metal then release device

Fig. 10 Integrated sensor fabrication process.

polysilicon sheet resistance after doping is 13 Ω/square. The polysilicon layer is then patterned to form the gates of the MOSFETs, the underneath electrodes of the transducer elements, and the interconnections between the elements and circuits (Fig. 10d). Polysilicon was chosen as the interconnect material due to the ease of patterning over the minimal topography at this point in the process, its moderately low resistance, and the fact that it is a shared layer. This latter feature eliminates the need for an additional contact layer as well.

After arsenic (120 KeV, 7×10^{15} cm^{-2}) implantation forms the n^+ source and drain regions of the MOSFETs, the sacrificial silicon dioxide layer (2.5 μm) is deposited on top of the patterned polysilicon. Bushing molds (small bumps on the underside of the second polysilicon layer to prevent it from intimate contact with the substrate) are opened in this oxide layer by a timed etch in buffered HF. Anchor and contact areas are also opened in this oxide layer as shown in Fig. 10e. At this point, a backside strip is performed to remove the deposited layers, leaving only the pad oxide layer remaining (Fig. 10e). Frontside structures are protected by a photoresist coating during the backside RIE etching.

The second polysilicon layer (2.5 μm thick) is then deposited by LPCVD. This polysilicon layer serves as both the structural material for the transducer elements and as local interconnect within the circuit regions. For this reason, it is heavily doped with phosphorus at 875° C for 420 min to achieve high conductivity (2.2 Ω/square). Another silicon dioxide layer (0.5 μm) is deposited and patterned by RIE. This oxide layer is used as a hard mask for the etch of the polysilicon film. It doubles as a passivation layer in the circuit regions (Fig. 10f).

To encapsulate the circuit areas during the release step, a trench is formed by etching away the first and second low-temperature oxide (silicon dioxide) (LTO) layers, exposing either the first silicon nitride or the first polysilicon layer (Fig. 10g). Next, a second silicon nitride layer (1200 Å) is deposited and patterned by plasma etching, opening the sensors and contact pads but covering the circuit area. The second nitride layer remains to protect the circuit from HF attack in the final release step (Fig. 10h).

After the etching of the second silicon nitride layer, a backside etch is performed to strip off the second nitride layer and the second polysilicon layer (Fig. 10h). The remaining pad oxide is removed from the backside by a wet etch. After the backside etch, a metal layer (500-Å Cr and 1000-Å Au) is deposited on the backside of the wafer for ohmic contact (Fig. 10i). The wafer is then diced and chips are immersed in HF (Fig. 10i) to complete the device fabrication. An SEM of a fabricated device is shown in Fig. 11.

C. CWRU/ADI Sensors

The CWRU/ADI shear stress sensor discussed in Sec. II.C. was fabricated by ADI in its first iMEMS™ process described in Refs. 17 and 18. Figure 12 is an SEM of the floating element. Note the comb fingers to the side of the transducer element and the large release holes throughout its surface.

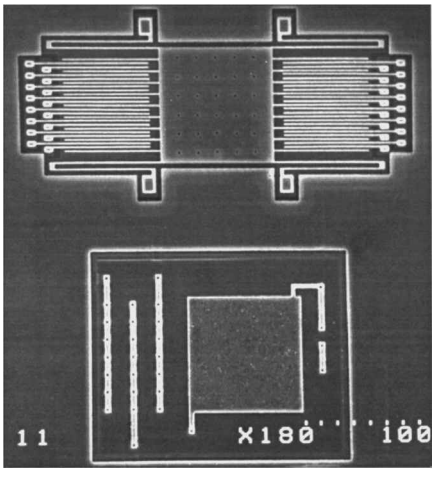

Fig. 11 SEM of a shear stress sensor showing transducer element and circuitry.

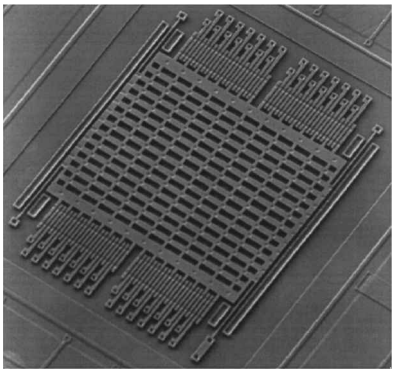

Fig. 12 CWRU/ADI shear stress sensor floating element.

IV. Conclusions

In this paper, the design and fabrication of floating-element shear stress microsensors by employing polysilicon-surface-micromachining and integrated circuit processing technologies is presented. Heavily phosphorus-doped polysilicon was used as the structural material to form microminiature floating elements suspended above a silicon substrate. The floating elements were attached to the substrate through folded-beam cantilever suspensions, forming the transducer elements of the sensors. The folded-beam suspension design was used because it relieved the residual stress in the deposited polysilicon layer. The deflection of the floating element can be measured either optically or through its capacitive coupling to horizontally interdigitated sense electrodes. Devices were developed with on-chip NMOS circuitry to provide an amplified output voltage with element deflection. In addition, active devices with signal-conditioning circuitry, which were designed to have a linear voltage response with respect to applied shear stress, were developed in cooperation with ADI.

Acknowledgments

This work was partially supported by NASA Lewis Research Center under Grant NAG3-1273. The authors thank Christopher A. Bang for the design of the floating element of the CWRU/ADI integrated sensor. Technical assistance from Microfabrication Laboratory staff and Electronics Design Center staff at Case Western Reserve University is greatly appreciated. Thanks to Jeff Melzak for assistance with the process development of the second-generation CWRU sensors. We thank Richie Payne at ADI for the opportunity to develop devices in the iMEMS™ run. Special thanks go to Brian Willis of NASA Lewis Research Center for his interest and for providing impetus to this research.

References

[1] Hyman, D., Pan, T., Reshotko, E., and Mehregany, M., "Microfabricated Shear Stress Sensors, Part 2: Testing and Calibration," *AIAA Journal,* Vol. 37, No. 1, 1999, pp. 73–78.

[2] Winter, K. G., "An Outline of the Techniques Available for the Measurement of Skin Friction in Turbulent Boundary Layers," *Progress in Aerospace Sciences*, Vol. 18, 1977, pp. 1–57.

[3] Hakkinen, R. J., "Survey of Skin Friction Measurement Techniques," AIAA Dayton-Cincinnati Section, 17th Annual Minisymposium on Aerospace Science and Technology, Dayton, OH, March 1991.

[4] Schmidt, M. A., "Microsensors for the Measurement of Shear Forces in Turbulent Boundary Layers," Ph.D. Thesis, Dept. of Electrical Engineering and Computer Science, Massachusetts Inst. of Technology, Cambridge, MA, 1988.

[5] Howe, R. T., Muller, R. S., Gabriel, K. J., and Trimmer, W. S., "Silicon Micromechanics: Sensors and Actuators on a Chip," *IEEE Spectrum*, Vol. 27, July 1990, pp. 29–35.

[6] Mehregany, M., "Microelectromechanical Systems," *IEEE Circuits & Devices*, Vol. 9, July 1993, pp. 14–22.

[7] Schmidt, M. A., Howe, R. T., and Senturia, S. D., "A Micromachined Floating-Element Shear Sensor," *The 4th International Conference on Solid-State Sensors and Actuators* (Tokyo, Japan), Inst. of Electrical and Electronics Engineers, 1987, pp. 383–386.

[8] Schmidt, M. A., Howe, R. T., Senturia, S. D., and Haritonidis, J. H., "Design and Calibration of a Microfabricated Floating-Element Shear-Stress Sensor," *IEEE Transactions on Electron Devices*, Vol. 35, June 1988, pp. 750–757.

[9]Shajii, J., Ng, K.-Y., and Schmidt, M., "A Microfabricated Floating-Element Shear Stress Sensor Using Wafer-Bonding Technology," *IEEE/ASME Journal of Microelectromechanical Systems*, Vol. 1, No. 2, 1992, pp. 89–94.

[10]Padmanabhan, A., Goldberg, H., Breuer, K., and Schmidt, M., "A Silicon Micromachined Floating-Element Shear Stress Sensor with Optical Position Sensing by Photodiodes," *Proceedings of Transducers '95* (Stockholm, Sweden), Vol. 2, Inst. of Electrical and Electronics Engineers, 1995, pp. 436–439.

[11]Liu, C., Tai, Y. C., Huang, J., and Ho, C. M., "Surface Micromachined Thermal Shear Stress Sensor," *Application of Microfabrication to Fluid Mechanics*, FED-Vol. 197, American Society of Mechanical Engineers, 1994, pp. 9–16.

[12]Huang, J., Ho, C. M., Tung, S., Liu, C., and Tai, Y. C., "Micro Thermal Shear Stress Sensor With and Without Cavity Underneath," *Proceedings of the IEEE Instrumentation and Measurement Technology Conference*, Inst. of Electrical and Electronics Engineers, Piscataway, NJ, 1995, pp. 171–174.

[13]Huang, J., Tung, S., Ho, C. M., Liu, C., and Tai, Y. C., "Improved Micro Thermal Shear Stress Sensor," *IEEE Transactions on Instrumentation and Measurement*, Vol. 45, No. 2, 1996, pp. 570–574.

[14]Tang, W. C., Nguyen, T. H., and Howe, R. T., "Laterally Driven Polysilicon Resonant Microstructures," *Sensors and Actuators A-Physical*, Vol. 20, Nov. 1989, pp. 25–32.

[15]Tang, W. C., Nguyen, T. H., Judy, M. W., and Howe, R. T., "Electrostatic-Comb Drive of Lateral Polysilicon Resonators," *Sensors and Actuators A-Physical*, Vol. 21, No. 1–3, 1990, pp. 328–331.

[16]Tang, W. C., "Electrostatic Comb Drive for Resonant Sensor and Actuator Applications," Ph.D. Thesis, Dept. of Electrical Engineering and Computer Sciences, Univ. of California, Berkeley, CA, 1990.

[17]"Data Sheet for ADXL50 Monolithic Accelerometer with Signal Conditioning," Analog Devices, 1994.

[18]Core, T. A., Tsang, W. K., and Sherman, S. J., "Fabrication Technology for an Integrated Surface-Micromachined Sensor," *Solid State Technology*, Vol. 26, Oct. 1993, pp. 39–47.

G. Laufer
Associate Editor